Characterisation of micro-Doppler due to the Horizontal antenna's Vibrations at Millimetre-Wave

Khalid A Al Mallak[1], Geoffery Hilton[1], Tian Hong Loh[2], Mark Beach[1]
[1] Communications Systems and Network, EPSRC CDT in Communications, University of Bristol (UoB)
Bristol, United Kingdom, {k.almallak, geoff.hilton, m.a.beach}@bristol.ac.uk
[2] Electromagnetic & Electrochemical Technologies Department, National Physical Laboratory/NPL,
Teddington, United Kingdom, tian.loh@npl.ac.uk

***Abstract*—This paper characterises the impact of horizontally induced vibration on the antenna's channel response due to fast vehicle manoeuvres or the side push of wind during the overtaking of a large vehicle on a motorway at millimetre wave (mmWave) frequencies. The resultant misalignment perturbs the point of observation, which produces Doppler shifts. A new composite antenna and channel model, including horizontal vibration within the antenna mounting, is developed by measuring the scattering parameters (S21) at discrete intervals of time using a vector network analyser (VNA) that generates a swept tone with a radio frequency (RF) measurement bandwidth of 2GHz centred at 25.5GHz. The S21 over discrete intervals of time represents the channel time-frequency transfer function which is utilised to generate the Doppler variant transfer function and the Doppler power spectrum after post-processing at a vibration frequency below 100Hz. It is proven experimentally that the induced Doppler power is directly proportional to the probability density function (PDF) of the Doppler Shifts. This indicates that Doppler shifts with high probabilities of occurrence have higher Doppler powers. For example, a Doppler shift ≤2000Hz having a PDF = 0.6 or above arrives with a higher power of up to -20dBm as compared to the Doppler shift of ±4000Hz, which has a lower PDF = 0.1 and Doppler powers ≤-25dBm.**

Keywords— Doppler power spectrum, Doppler shift, horizontal vibration, millimetre wave, time-frequency channel transfer function, vehicular channel.

I. Introduction

Micro-Doppler shift is the small Doppler shift shown due to the slow motion of an object or part of it, which is efficiently investigated in radar applications.

Millimetre-wave (mmWave) communications in 5G and beyond systems are beset with several implementation challenges that need to be resolved, especially for vehicular channels [1]. This is because the narrow antenna beamwidths, in which such systems become misaligned in azimuth and elevation or both, due to vibrations that occur, although the receiver's antenna is fixed to a vehicle's rigid body [2]. Furthermore, vibration produces phase noise varies with the vibration frequency as f_v^{-4} [3]. This degrades the received signal quality in the Vehicle-to-Infrastructure (V2I) and Vehicle-to-Vehicle (V2V) communications [4]. Moreover, such vibrations make the modelling of the composite antenna and channel response a key driver in mmWave research focusing on communications in moving platforms. However, in [5] a relationship between the antenna's vibration and a symbol error rate was proved based on the composite phase changes of the antenna's radiation pattern.

The Doppler shift and Doppler power spectrum can be used to characterise the vehicular channel. The horizontal vibration of the antenna generates a Doppler shift, as discussed in [6]. Consequently, filtering techniques discussed in [7] will be required to mitigate its impact. The antenna's vibration occurring due to suspension variations or from the engine whilst a vehicle is in motion is termed as vertical vibration, which the authors characterised, measured and proven in a vehicle [8]. However, horizontal vibrations can also occur during manoeuvres, turning or overtaking a large vehicle, which is the current paper's novelty. However, the relationship between Doppler shift and PDF of Doppler Power Spectrum has been proven for outdoor measurements using a 26GHz phased array antenna at Tx and a horn antenna at Rx [9]. The remainder of this paper is organised as follows. Section II presents the measurement setup. In Section III, the results are discussed. Finally, section IV concludes the paper.

II. Measurement Setup

A customised measurement system consisting of a stepper motor and Arduino controller is used to create horizontal vibrations, as illustrated in Fig. 1. The stepper motor is mounted on a rig perpendicular to the rotor shaft. The Arduino board is programmed using GCode to control the

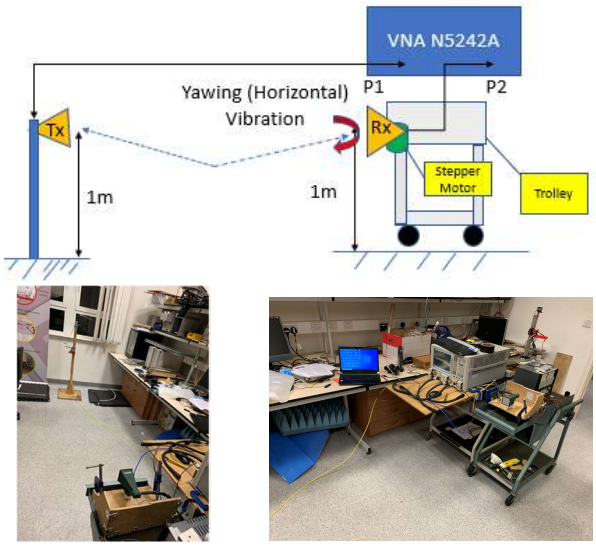

Figure 1: Shows a measurement\s setup diagram and underneath images taken from the Lab. Tx and Rx antennas are horizontally polarized.

Table I: Measurement's setup VNA parameters

Parameter (unit)	Value
Tx-Rx distance (m)	3
$h_{tx} - h_{rx}$ (m)	1
RF Bandwidth (GHz)	2
Centre frequency f_c (GHz)	25.5GHz
p_t (dBm)	5
Measurements time for one run (s)	28
No. of S_{21} snapshots recorded in one run	24
Time interval between each S_{21} snapshot (s)	1.16
Sweep frequencies samples	4001
Swep time τ (μs)	2

stepper motor such that it spins left and right constantly to produce the effect of horizontal vibration. A horn antenna is mounted vertically onto the stepper motor shaft using a suitable bearing. This is the receive (Rx) antenna, and this setup emulates a vehicular antenna mount and its horizontal vibration. Another horn antenna, which is the transmit (Tx) antenna, remains static as shown in the figure. Port 1 of a manually triggered vector network analyser (VNA) is connected to the Tx antenna, and Port 2 is connected to the Rx antenna. The VNA having an RF bandwidth of 2GHz generates a swept tone centreted at 25.5GHz. It records the scattering parameters (S21) over discrete intervals of time. In this way, induced vehicular motion due to horizontal vibrations is emulated and measured. Table I lists all parameters of the measurement setup.

The measurements are performed as (i) select two vital parameters of the stepper motor, namely the acceleration and the number of steps per millimetre from the GCode, (ii) run the Arduino script to produce Rx antenna's horizontal vibration, and (iii) simultaneously, the VNA records the S21.

A. Analysis of Stepper Motor Parameters

Two accelerations and steps per millimetre values are chosen for the stepper motor. They are 1500mm/s^2, 3000mm/s^2, 10steps/mm and 100steps/mm correspondingly, to create horizontal vibration at the Rx antenna. These values are used to compute the vibration frequency, explained as follows. First, the linear distance covered in 1s for the stepper motor acceleration of 1500mm/s^2 will be

Table II: Maximum & Minimum Doppler shifts (ν_m), radial velocity ($v(t)$) and vibration frequency (f_{vib}).

Acceleration = 1500mm/s^2	**step/mm = 10**	**step/mm = 100**
$v(t)$ (m/s)	70.7	7.07
ν_m (Hz)	±6126	±612.6
f_{vib} (Hz)	94.3	9.43
Acceleration = 3000mm/s^2	**step/mm = 10**	**step/mm = 100**
$v(t)$ (m/s)	141.4	14.14
ν_m (Hz)	±12252	±1225.2
f_{vib} (Hz)	94.3	9.43

$$x = \frac{1}{2}at^2 = \frac{1}{2} \cdot 1500 \cdot 1 = 750mm \quad (1)$$

Now, for the step value of 10steps/mm, the number of steps covered by the stepper motor in 750mm is $750\,\text{mm} \cdot 10\,\text{steps/mm} = 7500\,\text{steps}$. Next, the angle covered by the stepper motor in 10 steps will be $\frac{360^\circ}{10}$=36°. Therefore, the step angle, i.e., the angle by which the stepper motor rotates in one step, will be

$$step\ angle = \frac{36^\circ}{10} = 3.6^o \quad (2)$$

Thus the total angle the stepper motor rotates for 7500steps will be $7500 \cdot 3.6° = 27000°$. The radial velocity is now obtained as [10]

$$v(t) = total\ angle(rad) * L \quad (3)$$

Here, L is the length of the horn antenna, which is 15cm. Therefore, $v(t) = 27000 * \frac{\pi}{180} * 0.15 = 70.7$ m/s and the maximum Doppler shift will be $\nu_m = \pm\frac{f_c}{c} \cdot v(t) = \pm 6126$Hz, where $f_c = 25.5$GHz is the centre frequency and $c = 3 * \frac{10^8 m}{s}$ is the speed of light. Finally, the vibration frequency f_{vib} is computed as:

$$f_{vib} = v(t)/(total\ no.\frac{steps}{\frac{steps}{mm}}) \quad (4)$$

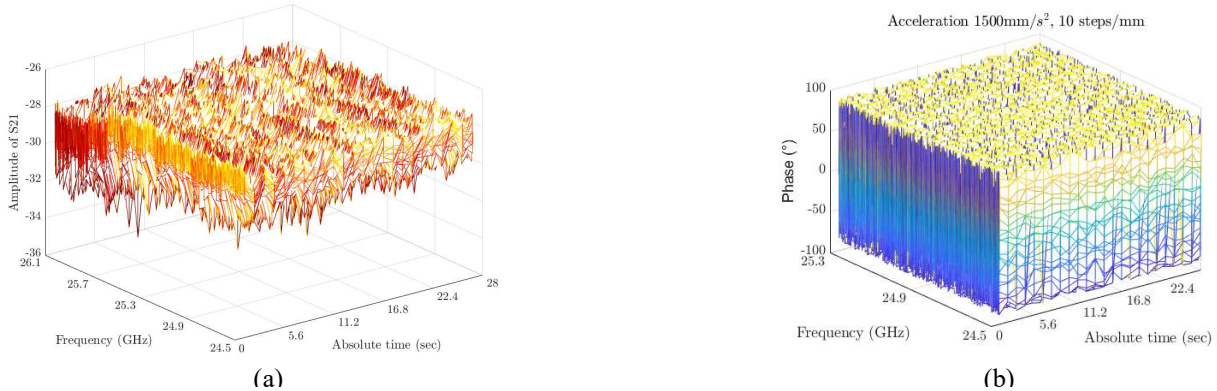

(a) (b)

Figure 2: (a) Amplitude response of the $|S_{21}(t,f)|$ and (b) phase response of the $\angle S_{21}(t,f)$ recorded for 28 seconds across an RF bandwidth of 2GHz. 24 discrete time snapshots are recorded. Hence, the time interval between each snapshot is 28seconds/24=1.167 seconds.

Hence, f_{vib} =70.7(m/s)/(7500steps/10steps/0.001m) = 94.3Hz. The same procedure can be applied to compute $v(t), v_m$ andf_{vib} for the stepper motor acceleration values of 3000mm/s^2 and 100 mm/s^2 as depicted in Table II, and not repeated herein. It is to be noted that as the step number increases by an order of magnitude from 10steps/mm to 100steps/mm, both the f_{vib} and maximum Doppler shift v_m reduce by an order of magnitude.

B. Time-Frequency Channel Transfer Function

The 24 discrete-time snapshots of the S21 across the RF bandwidth of 2GHz can be regarded as the time-frequency channel transfer function. The amplitude response of S21 is illustrated in Fig. 2(a) and the phase response in Fig. 2(b) for 7 such time snapshots. These discrete-time snapshots are collected for 28 seconds. Hence, the time interval between each snapshot is 28seconds/24 = 1.16seconds. Now, for the acceleration of 1500mm/s^2 at 10steps/mm, since the vibration frequency is computed as 94.3Hz (Table II), it stands to reason that within the time interval of 1.16seconds, the stepper motor (and hence the Rx antenna) vibrates 1.16·94.3=109.4 times. Therefore, each discrete time interval (of 1.16seconds) in Fig. 2 corresponds to a set of approximately 109 repeated angular positions of the Rx antenna. For each such repeated angular position of the Rx antenna, the associated amplitude and phase response of the S21 can then be extracted at all the 4001 frequency points within the 2GHz RF bandwidth span. This constitutes the true S21 amplitude and phase response. In Fig. 2(a), the peaks correspond to the amplitude variations along with the multipath components produced when the Rx antenna is misaligned with the Tx antenna (due to horizontal vibration).

Furthermore, In Fig 2(b), the horizontal vibration of the antenna causes the phase variation due to the difference between the axis of rotation and the phase centre of the Rx horn antenna. Lastly, the fluctuations in the RF cable (which attach the Rx antenna to Port 2 of the VNA) causes additional amplitude and phase variations. However, through separate cable measurements, it is determined that the variations in amplitude due to RF cable fluctuations is ≤ 0.5 dB. Additionally, these fluctuations will alter the true phase response to a certain extent. Therefore, whilst the variation in amplitude (≤ 0.5 dB) can be de-embedded from the S21 measurements, the additional phase variation persists, which is a limitation in our measurement setup.

C. Post Processing

The Fourier transform can be applied to the time-frequency channel transfer function to compute the Doppler variant transfer function as [5]

$$B(v,f) = \int_{-\infty}^{\infty} S_{21}(t,f)\exp^{-j2\pi v}\,dt \qquad (5)$$

where v is the Doppler shift, t are the discrete time snapshots and $24.5\text{GHz} \leq f \leq 26.5\text{GHz}$ are the swept frequencies within the RF bandwidth of 2GHz. The Doppler power spectrum $P_B(v)$ is now computed from the frequency cross-correlation of the Doppler variant transfer function $B(v,f)$ as

$$P_B(v,\Delta f = 0) = \int_{-\infty}^{\infty} B(v,f)\lceil B(v,f)\rceil df \qquad (6)$$

where $\lceil . \rceil$ indicates the ceiling function. The following section examines the relationship between the Doppler power

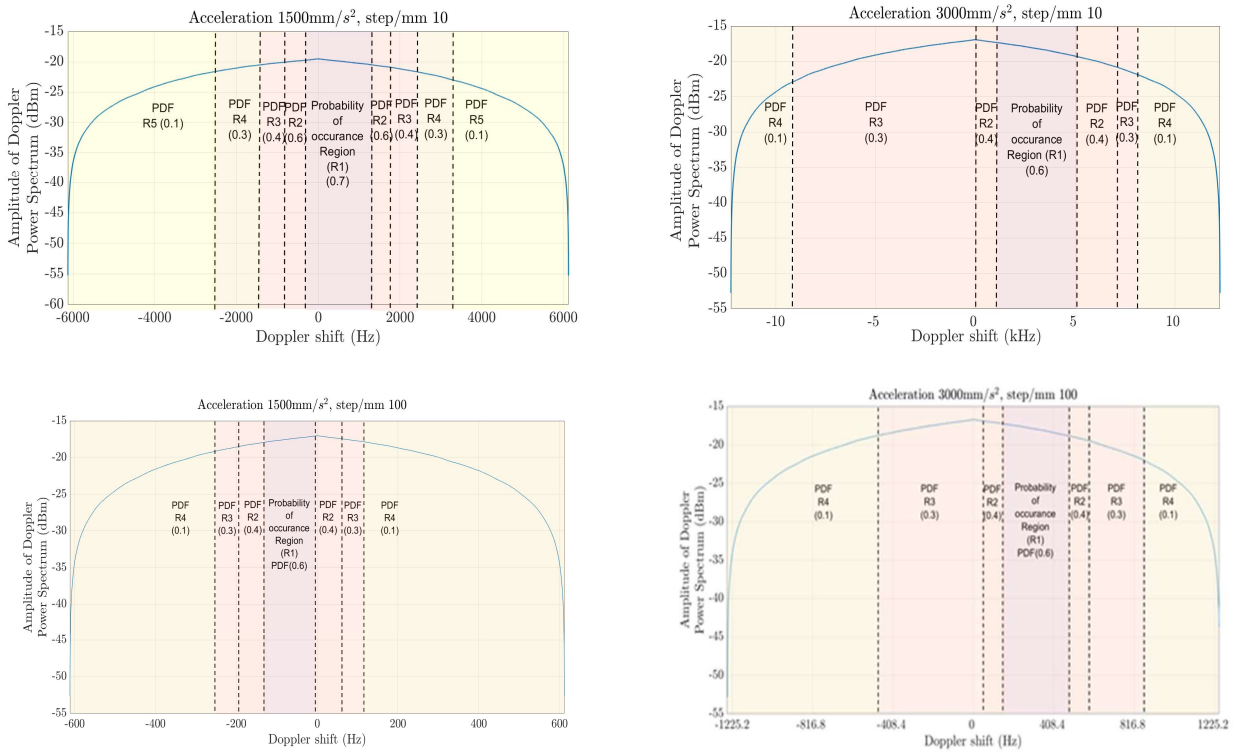

(a) (b)

Figure 3: P_B (v) against the Doppler shift for (a) 1500mm/s^2 and (b) 3000mm/s^2 accelerations with the the steps numbers 10mm/step (top) and 100mm/step (bottom).

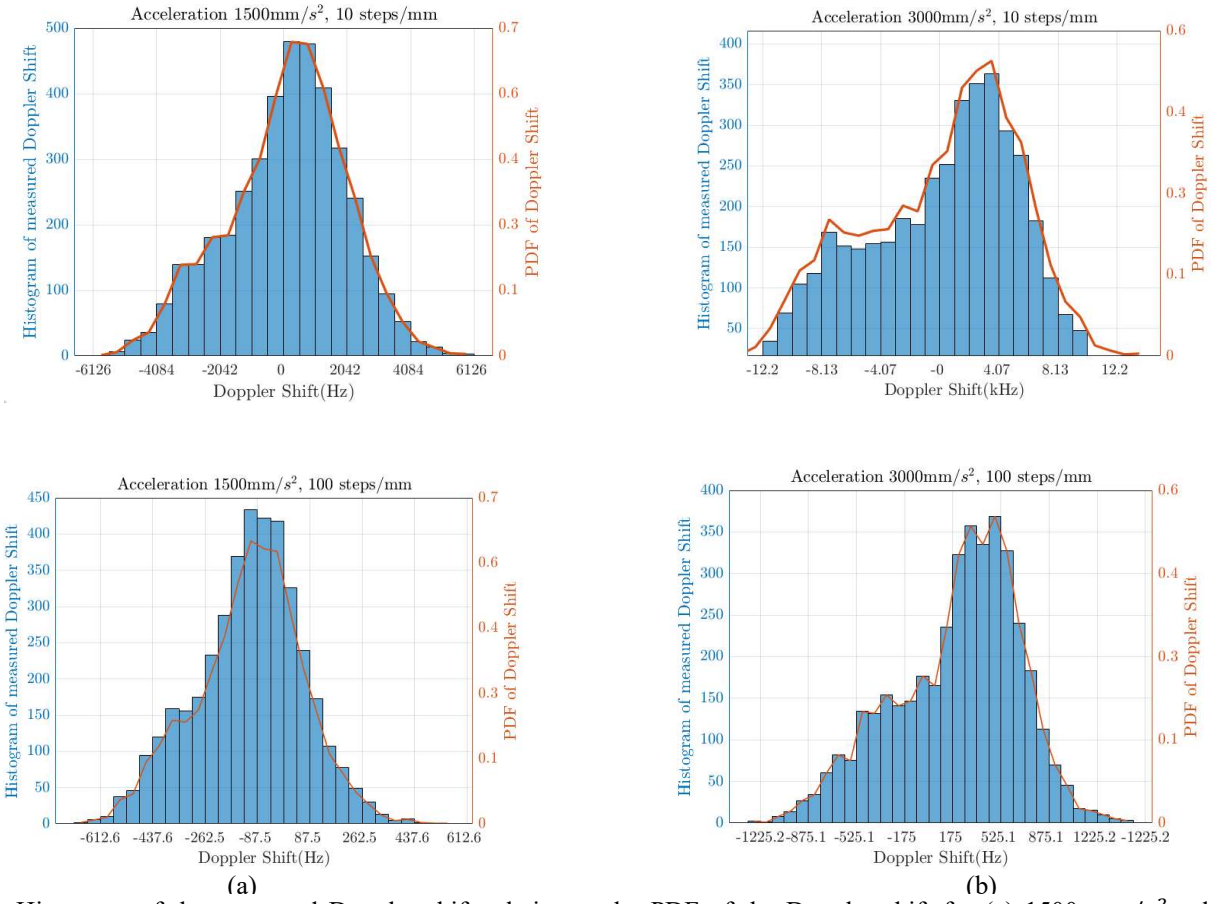

Figure 4: Histogram of the measured Doppler shift relative to the PDF of the Doppler shift for (a) 1500 mm/s^2 and (b) 3000 mm/s^2 at step numbers of 10mm/step (top) and 100mm/step (bottom).

spectrum and the PDF of the associated Doppler shifts in detail.

III. Results & Analysis

Fig. 3(a) and 3(b) plot the Doppler power spectrum $P_B(v)$ against the corresponding Doppler shifts v for the two stepper motor accelerations of 1500mm/s^2 and 3000mm/s^2 at the two steps/mm values of 10 and 100 correspondingly. These Doppler shifts are $v = \frac{v(t)}{c} \cdot f \cdot \cos(\theta - \theta_{v(t)})$ where $v(t)$ is the radial velocity as defined previously. It is observed that although the Doppler powers fall towards the extremities of the Doppler shifts (i.e., the peak Doppler powers have the lower Doppler shifts), their probabilities of occurrence vary, as illustrated in Fig. 3 depending upon their respective PDF values. For example, Region 1 (R1), containing the peak Doppler powers and lower Doppler shifts, have PDF values of 0.7 and 0.6 for the accelerations of 1500mm/s^2 and 3000mm/s^2 correspondingly. In other words, R1 is likely to occur the most. On the other hand, R5 containing the lower Doppler powers with the higher Doppler shifts having PDF values 0.1 are least likely to occur. It is also observed from Fig. 3 that increasing the step number by an order of magnitude from 10 to 100 tends to alter only those Doppler shift regions that have higher probabilities of occurrence, i.e., with the higher PDF values; whereas those Doppler shift regions with lower probabilities of occurrence (lower PDF vales) do not alter much. In addition, increasing the number of steps/mm for one acceleration results in decreasing the observed $P_B(v)$. However, the drop in $P_B(v)$ is very low (only 0.2dB) when the acceleration was doubled.

These PDF values are arrived at by ascertaining the exact nature of the relationship between the PDF of the Doppler shifts and the Doppler Power spectrum $P_B(v)$. First, the histogram of the Doppler shifts for the two accelerations and step values are obtained. From the histograms, the PDFs can be derived; which overlaid over the respective histograms are illustrated in Fig. 4. This procedure allows correlating the PDFs of the Doppler shifts to the respective Doppler shift regions in Fig. 3. For e.g., in Fig. 4(a) and Fig. 4(b), region R1 (PDF ≈ 0.7) contains lower Doppler shifts, and it is this region that is indicated by R1 in Fig. 3(a) and Fig. 3(b). Similarly, regions R2, R3, R4 and R5 with specific PDF vales and Doppler shifts observed from Fig. 4 are indicated in Fig. 3.

The PDFs indicate a largely Rician distribution of the Doppler shifts. This is due to a direct line-of-sight (LoS) channel between the Tx antenna and (the horizontally vibrating) Rx antenna. The PDF can be expressed as

$$p_\theta(\theta) = \frac{\theta}{\sigma^2} exp - \frac{\theta^2 + \theta_{RX,H}^2}{2\sigma^2} \qquad (7)$$

where θ is the angle-of-arrival (AoA) of the RF signal at the Rx antenna due to its horizontal vibration, $\left[-\frac{\theta_{RX,H}}{2}, \frac{\theta_{RX,H}}{2}\right]$ is

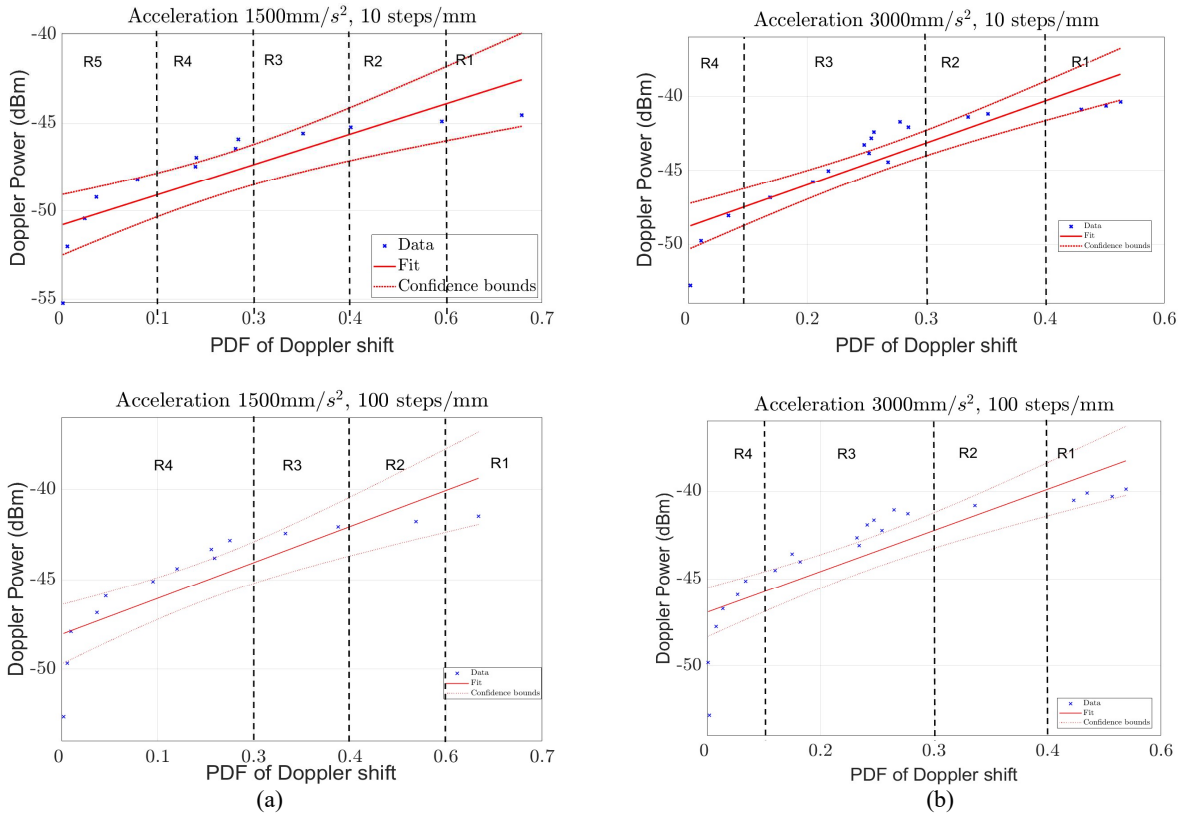

Figure 5: Proportionality of the Doppler power Spectrum with the PDF of the Doppler shift due to horizontal vibrations of the Rx horn antenna, for (a) 1500mm/s^2 and (b) 3000mm/s^2 at step number of 10mm/step (top) and 100mm/step (bottom). The Doppler powers are directly proportional to the PDF of the Doppler shifts indicating that larger Doppler powers have higher Doppler shifts.

the AoA range, and σ is the standard deviation of the AoA. Upon reception of the RF signal by the vibrating Rx antenna, f will be shifted by a value of $\nu = \frac{v(t)}{c} \cdot f \cdot \cos\left(\theta - \theta_{v(t)}\right)$ as derived previously. Therefore, the AoA θ can be expressed as:

$$\theta = \theta_{v(t)} + \cos^{-1}\frac{c}{v(t)\cdot f}\nu \tag{8}$$

Furthermore, the PDF of the Rician distributed Doppler shift can be expressed as a function of the Doppler shift ν as

$$p_\nu(\nu) = p_\theta(\theta)\left|\frac{d\theta}{d\nu}\right| \tag{9}$$

Substituting (8) in (9), we obtain

$$p_\nu(\nu) = p_\theta\left\{\theta_{v(t)} + \cos^{-1}\frac{c}{v(t)f_c}\nu\right\}\left|\frac{d\left\{\theta_{v(t)}+\cos^{-1}\frac{c}{v(t)f_c}\nu\right\}}{d\nu}\right| \tag{10}$$

Upon utilising the expression for $p_\theta(\theta)$ in (7), (10) can be solved to derive the complete expression for the PDF of the measured Rician distributed Doppler shift as a function of the Doppler shift ν, as given by

$$p_\nu(\nu) = \frac{1}{\sigma^2}\frac{\left\{\theta_{v(t)}+\cos^{-1}\frac{\nu}{\nu_m}\right\}\exp\frac{-1}{2\sigma^2}\left[\theta_{v(t)}+\cos^{-1}\frac{\nu}{\nu_m}\right]}{\nu_m\sqrt{1-\left(\frac{\nu}{\nu_m}\right)^2}} \tag{11}$$

where $\nu_m = \frac{v(t)}{c}\cdot f$, is the maximum Doppler shift as derived previously.

Since (i) the measurement scenario depicted in Fig. 1 is LoS and (ii) the Tx/Rx horn antenna patterns are sufficiently flat within their half-power beamwidths (HPBWs), the Doppler power spectrum $P_B(\nu)$ can be considered to be proportional to the PDF of the Rician distributed Doppler shift $p_\nu(\nu)$, further affected by the Rx antenna gain $G(\theta)$ (expressed as a function of the Doppler shift ν) [11]. It should be noted that the Doppler power spectrum $P_B(\nu)$ can also be derived directly from the Fourier Transform of the Doppler variant transfer function given in Equation (5). Hence, we write

$$\begin{aligned} P_B(\nu) &= \int_{-\infty}^{\infty} B(\nu, f)\exp -j2\pi\nu\, df \\ &= p_\nu(\nu)G(\theta) \\ &= \frac{G\left(\theta_{v(t)}+\cos^{-1}\frac{\nu}{\nu_m}\right)}{\sigma^2\nu_m\sqrt{1-\left(\frac{\nu}{\nu_m}\right)^2}}\exp\frac{-1}{2\sigma^2}\left[\theta_{v(t)}+\cos^{-1}\frac{\nu}{\nu_m}\right] \end{aligned} \tag{12}$$

Equation (12) shows the proportionality of the Doppler power spectrum $P_B(\nu)$ with the PDF of the Rician Doppler shift $p_\nu(\nu)$. Further, it indicates that the Rx horn antenna's gain $G(\theta)$ affects the Doppler power spectrum. $G(\theta)$ can be computed relative to the wavelength and aperture of the horn antenna [12].

Fig. 5 shows the linear regressions performed on the Doppler power spectrum $P_B(\nu)$ relative to their PDFs $p_\theta(\theta)$ (for the stepper motor accelerations of 1500mm/s^2 and 3000mm/s^2 at step values of 10steps/mm and 100steps/mm). The data fit proves the proportionality of the Doppler power spectrum and the PDFs of the Doppler shifts. The physical significance is that those Doppler shifts that have higher

PDFs also tend to have higher Doppler powers. However, the uncertainty tends to increase at lower PDF values, as depicted by the 95% confidence bounds. Such Doppler shifts are least likely to occur (and are associated with lowest Doppler powers). In order to investigate this phenomenon of higher uncertainty at low PDFs, in Fig. 5, the regions of PDF intervals R1, R2, R3, R4 (for the accelerations of 1500mm/s^2 and 3000mm/s^2) and R5 (for 1500mm/s^2 only) are once again depicted. In region R5 (Fig 5(a)) as well as R4 (Fig. 5(b)), the tail of the data does not nearly follow the straight-line fit and the proportional relationship between the Doppler powers and the PDFs of the associated Doppler shifts degenerates. Here again, the physical significance can be inferred by noting that R5 and R4 correspond to the Doppler shift extremities in Fig. 3(a) and 3(b), respectively, where the stepper motor abruptly starts or stops its motion (also indicated by the drastic fall in Doppler powers). In the rest of the regions (R1, R2, R3, R4 in Fig. 5(a), and R1, R2, R3 in Fig. 5(b)), however, the proportionality (of Doppler powers to the PDFs of the corresponding Doppler shifts) holds since the data is highly correlated which generates a straight line fit. The observations inferred can be summarised as follows.

- In mmWave vehicular channels, horizontal vibrations cause antenna's depointing. It will perturb the composite amplitude and phase of the radiation pattern. The phase changes are significant, as they add modulation at the receiver's side, which degrades the fidelity of the link and its information caring capacity.
- The proportional relationship between the Doppler power spectrum and the PDFs of the Doppler shifts is retained irrespective of the doubling of the stepper motor acceleration or the increase in the step number by an order of magnitude.
- Doubling the stepper motor acceleration doubles the maximum Doppler shift. Also, increasing the step number by an order of magnitude reduces the maximum Doppler shift by an order of magnitude. However, the amplitude of $P_B(v)$ decreases when steps per mm increase by an order of 10. Further, the implication in a vehicular channel is that (i) the Doppler shift doubles when the acceleration produced by the horizontal vibration doubles, and (ii) the Doppler shift reduces by the same order of magnitude as the increase in horizontal vibration frequency.
- The proportional relationship degenerates only in regions of abrupt start or stop of vibration and is accompanied by a sharp fall in the Doppler powers.

In other words, regions with Doppler powers of any consequence are highly correlated with and directly proportional to the PDFs of their associated Doppler shifts.

IV. Conclusions

This research characterised the impact of the antenna's horizontal vibrations on a vehicular channel at the mmWave frequency of 26GHz. The channel was emulated through a vibration rig implemented in a laboratory-based measurement setup. The time-frequency channel transfer function was recorded. Based on the given stepper motor parameters, the relationship of the Doppler power spectrum and the PDFs Doppler shifts generated due to the Rx antenna's horizontal vibrations were investigated. It was proven that the Doppler powers are proportional to the PDF of the Doppler shifts for a horizontally vibrated antenna. The highest Doppler powers of up to -20dBm (Doppler shifts $\leq$ 2000Hz, stepper motor acceleration of 1500steps/mm^2) and -10dBm (Doppler shifts $\leq$ 1250Hz, acceleration of 3000steps/mm^2) tend to occur the most and has the highest PDF values of 0.7 and 0.6 respectively. These results conclusively establish the dependency of induced the Doppler power spectrum on the PDF of Doppler shifts occurring due to the Rx antenna's horizontal vibrations in the Lab.

References

[1] F. Fuschini *et al.*, "Analysis of In-Room mm-Wave Propagation: Directional Channel Measurements and Ray Tracing Simulations," *Journal of Infrared, Millimeter, and Terahertz Waves,* vol. 38, no. 6, pp. 727-744, 2017/06/01 2017, doi: 10.1007/s10762-017-0366-1.

[2] M. Soliman, Y. Dawoud, E. Staudinger, S. Sand, A. Schuetz, and A. Dekorsy, "Influences of train wagon vibrations on the mmwave wagon-to-wagon channel," in *12th European Conference on Antennas and Propagation (EuCAP 2018)*, 9-13 April 2018 2018, pp. 1-5, doi: 10.1049/cp.2018.0962.

[3] J. S. Ward, "Phase Noise Induced by a Vibrating Antenna," *IEEE Transactions on Microwave Theory and Techniques,* vol. 65, no. 11, pp. 4148-4153, 2017, doi: 10.1109/TMTT.2017.2699682.

[4] M. Brambilla, M. Nicoli, S. Savaresi, and U. Spagnolini, "Inertial Sensor Aided mmWave Beam Tracking to Support Cooperative Autonomous Driving," in *2019 IEEE International Conference on Communications Workshops (ICC Workshops)*, 20-24 May 2019 2019, pp. 1-6, doi: 10.1109/ICCW.2019.8756931.

[5] H. Mingchao, Z. Pengbo, L. Haoyan, S. Guoliang, and J. Shuqiang, "Performance Analysis of Wireless Communication System Affected by Vibrating Antenna," in *2020 IEEE 20th International Conference on Communication Technology (ICCT)*, 28-31 Oct. 2020 2020, pp. 858-862, doi: 10.1109/ICCT50939.2020.9295692.

[6] V. C. Chen, F. Li, S. Ho, and H. Wechsler, "Micro-Doppler effect in radar: phenomenon, model, and simulation study," *IEEE Transactions on Aerospace and Electronic Systems,* vol. 42, no. 1, pp. 2-21, 2006, doi: 10.1109/TAES.2006.1603402.

[7] D. Belgiovane and C. Chen, "Micro-Doppler characteristics of pedestrians and bicycles for automotive radar sensors at 77 GHz," in *2017 11th European Conference on Antennas and Propagation (EUCAP)*, 19-24 March 2017 2017, pp. 2912-2916, doi: 10.23919/EuCAP.2017.7928457.

[8] K. A. A. Mallak, M. Nair, G. Hilton, T. H. Loh, and M. Beach, "Characterising Vehicle Suspension Variations in Millimetre Wave V2I System," in *2021 IEEE 93rd Vehicular Technology Conference (VTC2021-Spring)*, 25-28 April 2021 2021, pp. 1-5, doi: 10.1109/VTC2021-Spring51267.2021.9448901.

[9] K. A. A. Mallak, M. Nair, G. Hilton, T. H. Loh, and M. A. Beach, "Characterising the Impact of Antenna Beamwidth on the Performance of Vehicle-to-Infrastructure (V2I) Millimetre Wave Communication," in *2021 International Symposium on Networks, Computers and Communications (ISNCC)*, 31 Oct.-2 Nov. 2021 2021, pp. 1-6, doi: 10.1109/ISNCC52172.2021.9615843.

[10] Y. Balal, N. Balal, Y. Richter, and Y. Pinhasi, "Time-Frequency Spectral Signature of Limb Movements and Height Estimation Using Micro-Doppler Millimeter-Wave Radar," *Sensors,* vol. 20, no. 17, 2020, doi: 10.3390/s20174660.

[11] L. Wang *et al.*, "Vehicle-to-infrastructure channel characterisation in urban environment at 28 GHz," *China Communications,* vol. 16, no. 2, pp. 36-48, 2019.

[12] J. Lorca, M. Hunukumbure, and Y. Wang, "On Overcoming the Impact of Doppler Spectrum in Millimeter-Wave V2I Communications," in *2017 IEEE Globecom Workshops (GC Wkshps)*, 4-8 Dec. 2017 2017, pp. 1-6, doi: 10.1109/GLOCOMW.2017.8269039.